THE AMERICAN SOCIETY OF MECHANICAL ENGINEERS
345 E. 47 St., New York, N.Y. 10017

92-G

Numerical Simulation of Compressor Endwall and Casing Treatment Flow Phenomena

A. J. CROOK
Allison Gas Turbine Division
Indianapolis, IN

E. M. GREITZER, C. S. TAN
Massachusetts Institute of Technology
Cambridge, MA

J. J. ADAMCZYK
NASA Lewis Research Center
Cleveland, OH

ABSTRACT

A numerical study is presented of the flow in the endwall region of a compressor blade row, in conditions of operation with both smooth and grooved endwalls. The computations are first compared to velocity field measurements in a cantilevered stator/rotating hub configuration to confirm that the salient features are captured. Computations are then interrogated to examine the tip leakage flow structure since this is a dominant feature of the endwall region. In particular, the high blockage that can exist near the endwalls at the rear of a compressor blade passage appears to be directly linked to low total pressure fluid associated with the leakage flow. The fluid dynamic action of the grooved endwall, representative of the casing treatments that have been most successful in suppressing stall, is then simulated computationally and two principal effects are identified. One is suction of the low total pressure, high blockage fluid at the rear of the passage. The second is energizing of the tip leakage flow, most notably in the core of the leakage vortex, thereby suppressing the blockage at its source.

INTRODUCTION

It is well known that the use of grooves or slots in the endwall of a compressor can substantially increase the stable flow range of the machine, although generally with some penalty in efficiency (e.g. Prince, Wisler and Hilvers, 1977; Fujita and Takata, 1984; Smith and Cumpsty, 1985). Such grooves have been successfully employed in a variety of different geometries and flow regimes: over rotor tips in both high and low Mach number axial compressors, on a rotating hub under a cantilevered stator, in an axial compressor, and over the impeller, as well as on a rotating shroud under a vaned diffuser in a centrifugal compressor. Several current engines, in fact, make use of this "casing treatment".

There have been a number of investigations to assess performance of compressors with grooved endwalls, but the basic fluid mechanics underlying the increased ability of the blade row to withstand stall is still not well understood. One reason is that, even with a smooth shroud or hub, the flow in the endwall region of a compressor blade is complex. More precisely, simplifying approaches which have worked well in other realms of fluid dynamics (e.g. secondary flow, boundary layer analyses) have not been helpful in providing the required insight.

As will be argued below, although our original interest was in the mechanism of operation of casing treatment, it became evident that better understanding of the flow with a smooth endwall was a prerequisite for dealing with grooved endwall configurations. The paper thus presents an examination of both of these situations, with the central focus on flow structure in the endwall region with a tip, or hub, clearance. From considerations of this structure, possible mechanisms are presented not only for compressor stall but for its delay when a grooved endwall is used.

BACKGROUND OF RESEARCH ON CASING TREATMENT

As background, we present a brief description of the features of compressor casing treatment which are relevant to the investigation reported herein. First, it has been shown that casing treatment is effective only in situations in which the flow in the endwall region sets the stall limit, i.e. wall stall or endwall stall (Greitzer et al., 1979; MacDougall, 1988); this is the case in the configuration studied here. In addition, we concentrate on those treatments that have had the most success in suppressing stall, namely the so-called "axial skewed grooves", which have been examined by other investigators, most notably Smith and Cumpsty (1985), and Takata and co-workers (1977, 1984). The axial skewed grooves used in the experiments to be discussed are depicted in Fig. 1. An important aspect of the flow in these grooves is the recirculation, from the rear of the passage to the front, driven by the mean pressure rise of the compressor. Although the recirculation is unsteady (because a given groove sweeps through the pressure field of the blades), the unsteady effects have been shown by Smith and Cumpsty (1985) to be of secondary importance, so that it is the mean, back-to-front, motion that is critical.

The recirculation through the groove has two main consequences for the flow in the passage: removal of fluid at the rear, and injection of fluid at the front. Because of the relative motion of the groove and the blade, there is work done as the fluid passes through the groove and the injected fluid usually enters with a higher than free stream total pressure in the blade relative frame.

Lee and Greitzer (1990) have assessed the influence of injection and removal on stall inception by independently varying the

Presented at the International Gas Turbine and Aeroengine Congress and Exposition
Cologne, Germany June 1-4, 1992
This paper has been accepted for publication in the Transactions of the ASME
Discussion of it will be accepted at ASME Headquarters until September 30, 1992

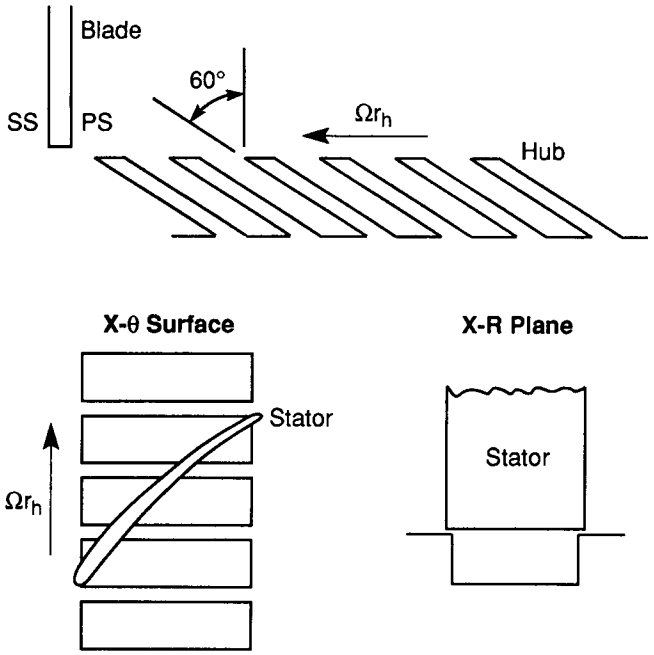

Fig. 1: Detail of hub treatment used in experiment (geometry similar to rotor casing treatment)

rate and the position of the two. In this manner, the effect of each could be examined separately. Both injection and removal were found to be useful in delaying stall, although neither was as effective by itself as the casing treatment in which they both act in combination. For injection, a strong correlation was found between change in stalling pressure rise capability and streamwise component of momentum of the injected flow.

While one might infer that *removal* is analogous to boundary layer suction, i.e, sucking off the low velocity flow near the endwall, there are differences between the flow with a moving endwall (even a smooth one) and a conventional boundary layer. In particular, as pointed out by Smith and Cumpsty (1985), Lee (1988), and Johnson (1985), the fluid that exists at locations toward the rear of the passage has a relative dynamic pressure which is a sizeable fraction of the free stream dynamic pressure. In fan rotors, for example, where much of the high speed work on casing treatment has been carried out, the stagger angles may be sixty-five degrees or more. For these geometries, the relative dynamic pressure of the fluid *on* the wall is over eighty percent of the free stream value at inlet. Since the relative velocity decreases through the rotor along a streamline away from the wall, this ratio is even higher at exit, and it is not obvious why removing this high dynamic pressure fluid would delay stall.

The situation with *injection* at the front of the blade passage is even less resolved. A link between increase in pressure rise capability and streamwise momentum addition certainly seems plausible. However, even a qualitative description of the interaction between the injected and the blade passage flow which is responsible for this link was lacking when this study was initiated.

With the foregoing as background, we pose the two fluid dynamic issues to be addressed in this paper:

1) What is the mechanism of stall with a smooth wall, i.e. what features of the flow in the endwall region set the limit on pressure rise capability?
2) How does casing or hub treatment act to alleviate these consequences?

MOTIVATION AND SCOPE OF THE PAPER

It is useful to discuss briefly the objectives of the present investigation, since these determined the underlying approach. Although a number of different approximate approaches to the compressor endwall problem have been tried and found wanting, in the past few years, numerical procedures have been developed that can capture the basic "flow physics" of realistic configurations (e.g. Hah, 1986; Pouagare and Delaney, 1986; Dawes, 1987; Adamczyk, 1989). We have used one such procedure (Adamczyk, 1989) to examine the endwall regionflow structure, for smooth and grooved endwalls. The emphasis of the study is not on precise prediction of loss levels or deviation for a specific geometry, but rather on using computations to develop understanding of phenomena that occur in a broad class of turbomachines which use casing treatment. The question to be asked of the numerical procedures is therefore whether they are able to capture those features of the endwall/tip clearance flow that have a major impact on these phenomena. As seen below, our position is that the answer to the question is yes, and that one can derive considerable physical insight from interrogation of the computational results.

The organization of the paper, which reflects these views, is thus somewhat unconventional in that comparison with experiment is presented at an early stage, essentially as part of the methodology rather than the results. We first summarize the computational procedure. The experimental configuration is then described, and a discussion is given of the modifications made to the computation to simulate the grooved endwall. Comparison of the numerical solutions with measurements is then presented, as illustration of the ability of the computations to reproduce experimental results for endwall flow, with a smooth wall and with an axial skewed groove configuration. The degree to which salient features are captured gives confidence that the computation can be used to probe other key aspects of the flow. We therefore examine in more detail the tip clearance velocity and total pressure fields, and the streamlines at various locations in the endwall region, for both smooth and grooved walls. From the computational results, it will be seen that there is a close link between the tip leakage flow and the high loss, high blockage, region at the rear of the blade passage, and that the action of the casing or hub treatment is to decrease this blockage through energizing of the leakage vortex core region.

BRIEF DESCRIPTION OF THE COMPUTATIONAL PROCEDURE

The computational scheme is based on a finite volume-time marching procedure, originally developed by Jameson (1981). The scheme is finite volume-cell centered and is second order accurate in space for a smooth uniform mesh. The time-stepping scheme is a four-stage Runge-Kutta integration, with local time stepping for each cell used to accelerate convergence. Further description of the scheme is given in the Appendix.

The boundary conditions at upstream and downstream ends of the computational domain, as well as on the blade and the smooth endwall, are standard for these types of three-dimensional codes. The total pressure profile used at inlet was the one measured in the experiment. Additional information on the computational procedure and boundary conditions can be found in Crook (1989).

EXPERIMENTAL CONFIGURATION USED TO ASSESS THE COMPUTATIONAL RESULTS

The experimental measurements were made in a single-stage low speed compressor facility. The endwall region examined was at the *rotating hub* of a *cantilevered stator*. The stagger of the rotor and

the stator, and the stator hub clearance, were chosen so that the stator hub would be the stalling section and the flow at this section would be similar to that at the tip of a compressor rotor. The overall performance, as well as the detailed measurements, show that this is the case and that the stator/rotating hub configuration gives a useful simulation of the flow phenomena occurring at rotor tips. This last point should be stressed, since it is the generic aspects of the measurements (and of the computations) that are of most interest. The stator operating point was at a high loading condition, close to the peak pressure rise point. Further information on the overall performance (pressure rise versus flow) of the stator row with and without the grooved hub are given by Cheng et al. (1984), and Lee and Greitzer (1990). Detailed measurements were also carried out on the three-dimensional flow in the stator passage using hot wires, and these are described in the latter of the above references and by Johnson (1985).

SIMULATION OF HUB TREATMENT IN THE COMPUTATIONS

The hub treatment grooves in the experiments extended from five to ninety-five percent axial chord, as illustrated in Fig. 1. The groove design was taken from geometries which have shown large stall margin increases when used as rotor casing treatment. The flow from the grooves is unsteady, but the measurements of Johnson (1985) indicate that the discrete jets out of the grooves mix rapidly. In particular, except in the first ten percent of chord and the bottom several percent of the span, time resolved measurements showed little deviation from time averaged data. Based on these experiments, steady-state simulation of the hub treatment was adopted.

Hub or casing treatments have an area of flow removal over the downstream portion, and an area of flow injection over the upstream portion, of the treatment area, as indicated in Fig. 2, which shows the radial component of velocity, V, non-dimensionalized by the stator mean axial velocity, $\bar{C}_x$. This combination of flow removal and injection can be simulated numerically by modeling the treatment area as a second inlet/exit to the flowfield domain. The four conditions specified at the boundary of the hub treatment (see Fig. 3) were the r-z flow angle, the r-θ flow angle, the stagnation temperature, and the radial mass flow (density and radial velocity). The r-z flow angle was set at zero and the r-θ angle was calculated assuming that the flow in the grooves had a relative angle equal to the angle of the treatment, as shown in Fig. 3. From the data of Johnson (1985) and

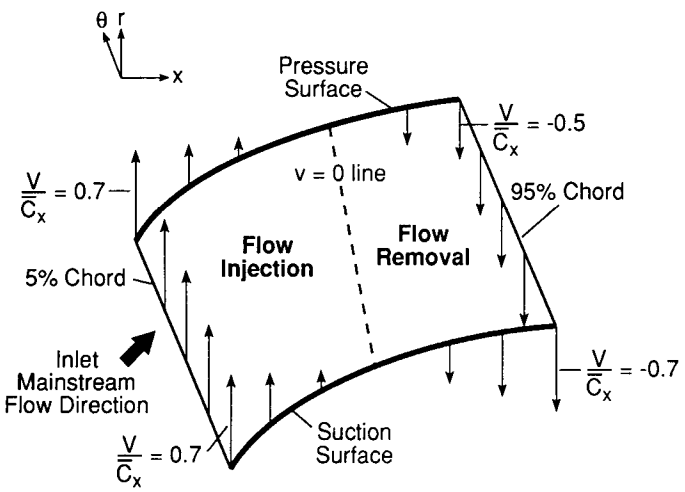

Fig. 2: Hub treatment radial velocity profile; V denotes radial velocity

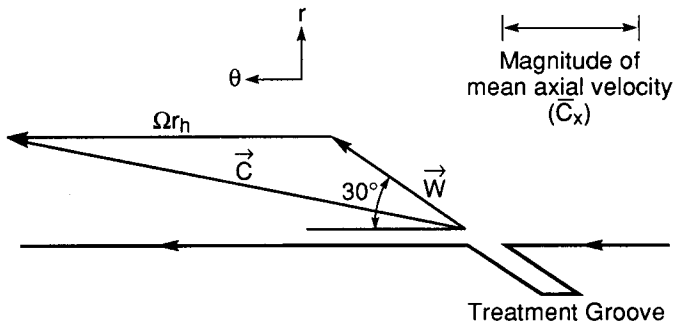

Fig. 3: Relative and absolute velocity vectors at treatment exit

Smith and Cumpsty (1982), the shape of the radial velocity near the hub is roughly a saw-tooth as a function of axial distance. The magnitude of the radial velocity was set by prescribing the amount of flow injected (or removed, since the two must balance) to be 3.5 percent of the inlet mass flow, which was the measured value.

COMPARISON OF NUMERICAL SOLUTIONS TO EXPERIMENTS

Velocity measurements were taken at seven radial locations in the hub region of the blade passage. The first station was at two percent span, the location corresponding to the end of the blade, i.e. the top of the clearance, and the outermost was at twenty-seven percent. Each radial station had seventy-six data points spaced evenly between the blades. For the comparisons to be presented, the velocities from the numerical solution grid were interpolated to the experimental locations unless otherwise specified.

The velocity data are organized in two types of surfaces, one at constant radius and one at constant axial station. For the latter, the angle at which the velocity vectors are viewed is important in extracting the flow structure. The view angle used, unless stated, is the stagger angle of the blades. Although no one angle is totally satisfactory because of the variation in flow angle with radius, and although more elaborate schemes can be used for bringing out the "secondary flow" aspects, viewing along the stagger angle can be thought of as roughly viewing along the free stream direction. The effect of viewing angle on the observed flow pattern is shown by Crook (1989); it is analogous to the imposition of a constant (cross-flow) velocity. If the latter is large, information about any circulatory or vortical structure tend to be submerged, so that the flow appears roughly unidirectional.

COMPARISON OF SMOOTH WALL RESULTS

Velocity vectors at two percent span, the radial measurement location closest to the endwall, are shown in Fig. 4 for the smooth endwall. Experimental measurements and viscous and inviscid computations are presented to illustrate several points. First, the strong cross-flow, which is evident in the rear of the passage, is the result of the tip leakage. Second, both of the numerical solutions can be seen to reproduce the measured magnitude of the cross-flow as well as the axial extent, although the viscous solution gives better representation. Similarity between experiment and (the two) numerical solutions is also seen for the line demarcating the passage throughflow and the leakage cross-flow. We include the inviscid results to emphasize that the leakage flow is pressure driven and the computations are insensitive to details of the turbulence modelling used. Further evidence on the minor role played by turbulence

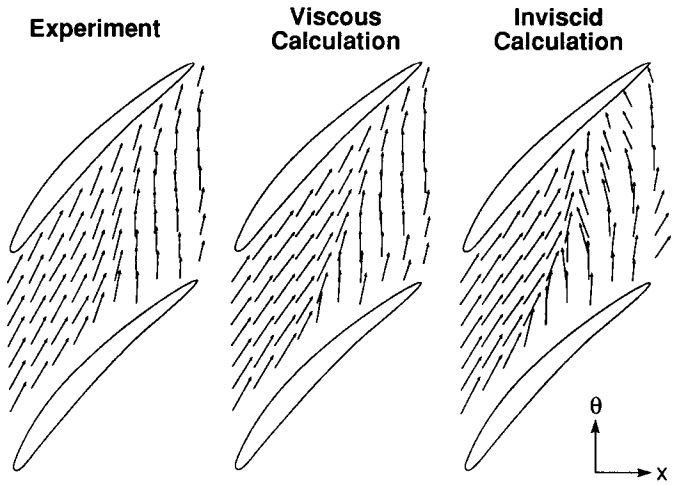

Fig. 4: Velocity vectors on surfaces of constant radius at 2% span from hub; for smooth wall

modelling considerations in this problem can be found in Crook (1989) and Storer (1991).

Good correspondence between experiment and numerical solution was also seen at other radial stations, but the clearance flow has the greatest effect at the two percent span location, and subsequent comparisons will focus on this station. In addition, because the viscous code was used in the hub treatment studies, we will show comparisons with viscous computations only from now on.

Velocity vector data are useful for showing overall similarity between computation and experiment, but numerical comparisons are more readily made if the data are displayed as contour plots. Figure 5 thus shows contour plots of velocity magnitude, C, referenced to the average inlet axial velocity, $\overline{C}_x$, for experiment and computations, again at the two percent span radial location. Agreement is seen between calculation and experiment in both magnitude and pattern.

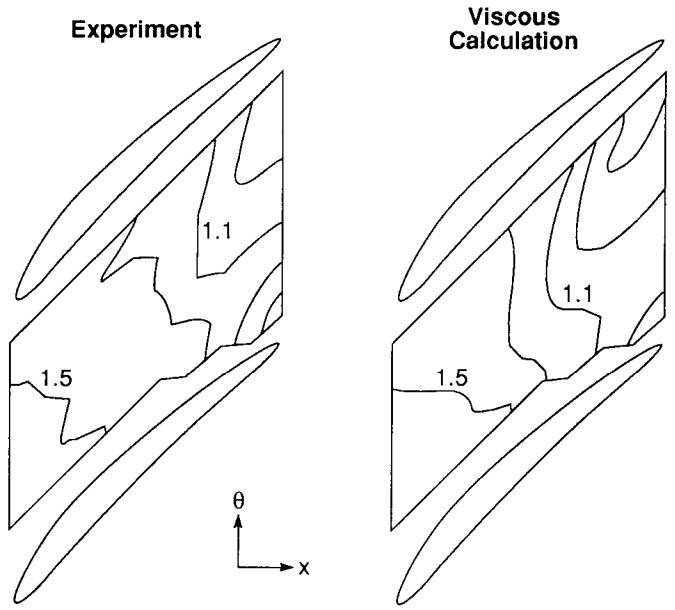

Fig. 5: Contours of $C/\overline{C}_x$ on constant radius surface at 2% span; for smooth wall

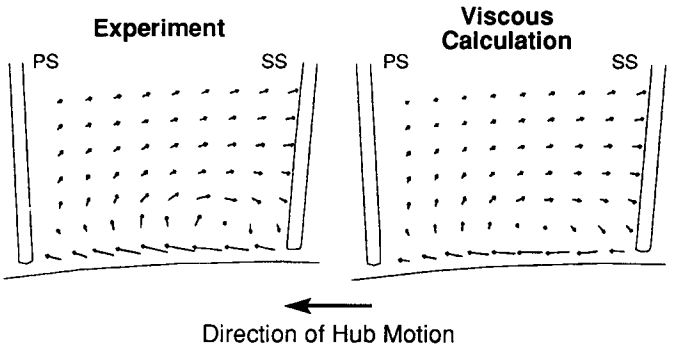

Fig. 6: Velocity vectors at 90% chord axial station for smooth wall

Figure 6 shows velocity vectors on axial planes at 90% chord, from experiment and from the numerical solution. The tip leakage flow from the blade at the right of the passage is evident. The leakage flow and its roll-up into a vortex are major features in the endwall region, and the numerical solution captures these features. Although only viscous results are shown, the strength of the clearance vortex in both viscous and inviscid numerical solutions is similar to experiment; the non-dimensional circulation (circulation divided by blade chord times mean axial velocity) was 0.68 in the experiment, 0.58 in the viscous calculation, and 0.79 in the inviscid calculation, again demonstrating the essentially inviscid nature of the leakage flow. The main difference between the three is the position of the vortex in the inviscid solution (Crook, 1989).

COMPARISON WITH HUB TREATMENT EXPERIMENTS

Velocity vectors on the radial surface at two percent span with hub treatment are shown in Fig. 7 for experiment and computation. In both, the jet flow from the forward portions of the treatment is considerably stronger than the clearance flow with the smooth wall.

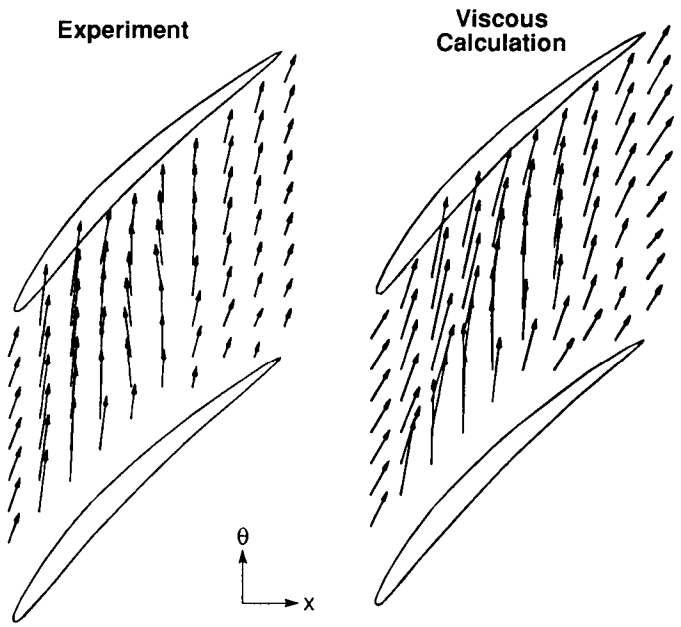

Fig. 7: Velocity vectors on constant radius surface at 2% span with hub treatment

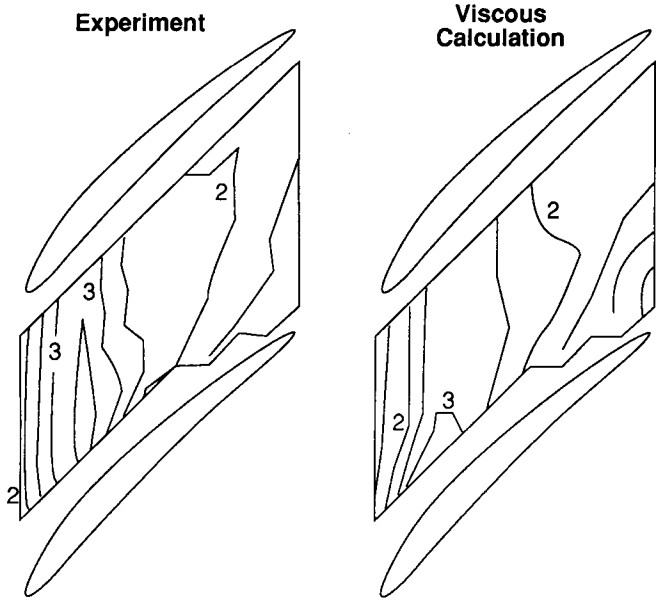

Fig. 8: Contours of velocity magnitude ($C/\overline{C}_x$) on constant radius surface at 2% span with hub treatment

Representative velocities with the hub treatment are roughly twice those associated with the smooth wall clearance flow, i.e. the dynamic pressure is roughly four times as high.

Contour plots of the normalized velocity magnitude ($C/\overline{C}_x$) for experiment and for computation, show similar patterns as seen in Fig. 8. The contour with magnitude greater than three, which outlines the hub treatment flow in the forward portion of the passage, can be compared with the values of one to one-and-a-half which existed with the smooth wall (Fig. 5).

Velocity vectors on an axial plane at 90% chord are displayed in Fig. 9. A downward velocity into the treatment exists in both experiment and numerical solution. A vortical structure is also seen in the left portion of the passage in both experiment and computation, although it is not precisely in the same place. (Note the slight shift in the positions of the interpolated calculation points.) The experimentally measured circulation was approximately twice that of the smooth wall; the computational value was 1.8 times that of the smooth wall. The changes in circulation compared to the smooth wall situation result from the vorticity in the treatment jet.

We can summarize the comparisons shown in Figs. 4 to 9 by stating that the major features in the endwall region, namely the

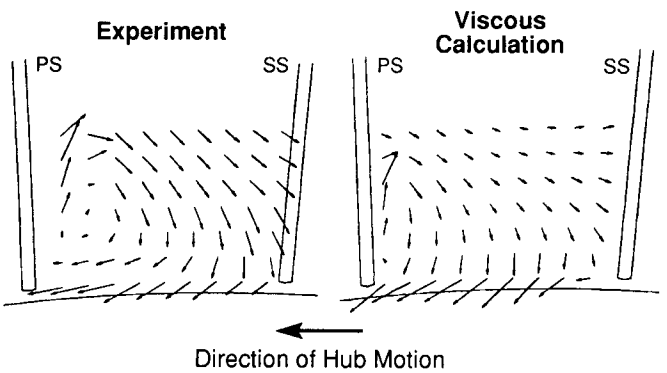

Fig. 9: Velocity vectors at 90% chord axial station with hub treatment

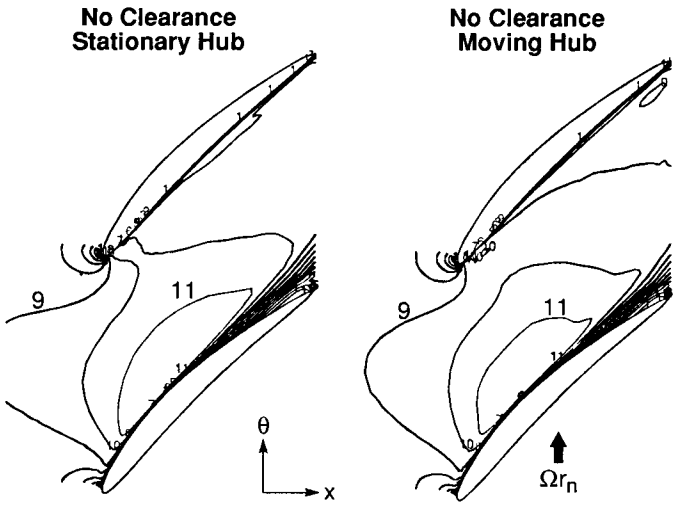

Fig. 10: Axial velocity ($C_x/\overline{C}_x$) on constant radius surface at 2.4% span for smooth wall (contour 1 = 0.0, contour 11 = 1.0, contour increment = 0.1)

clearance leakage cross-flow, the vortex associated with this leakage, and the large change in velocity field due to the high velocity jet emerging out of the treatment grooves, are well captured. (Crook (1989) shows that this was also true for the inviscid calculations, implying, as stated previously, that turbulence modelling plays little role in determining the degree to which the computations describe the principal flow features.) In addition, it should be emphasized that differences between experiment and computation are significantly less than those between smooth wall and hub treatment flows, and it is this latter comparison upon which we focus. The evidence, therefore, is that the computations can be used to examine aspects of the flow field other than those which can be measured experimentally. This is the main theme of the paper, and the one to which we now turn.

ANALYSIS OF NUMERICAL SOLUTIONS

The numerical solutions generated to investigate the endwall and hub treatment flow fields are listed in Table 1. The first two have no clearance and were carried out to illustrate the different effects of (a) moving endwall, and (b) clearance, separately.

TABLE 1
DESCRIPTION OF NUMERICAL SOLUTIONS

Solution #	Description
1	No clearance, smooth wall, stationary hub
2	No clearance, smooth wall, moving hub
3	Clearance, smooth wall, moving hub
4	Clearance, hub treatment

No Clearance/Smooth Wall/Stationary Hub

A feature of the flow with no clearance is a suction surface-hub corner separation. Figure 10a, which is a contour plot of the axial velocity normalized by inlet average axial velocity at 2.4% span, shows this. The conditions are that the endwall is stationary and there is no clearance. The increment between contour lines is 0.1 $\overline{C}_x$. A corner separation can be seen with a region of negative axial velocity near the trailing edge; the separation is similar to that found by Dong et al. (1986), although smaller in extent.

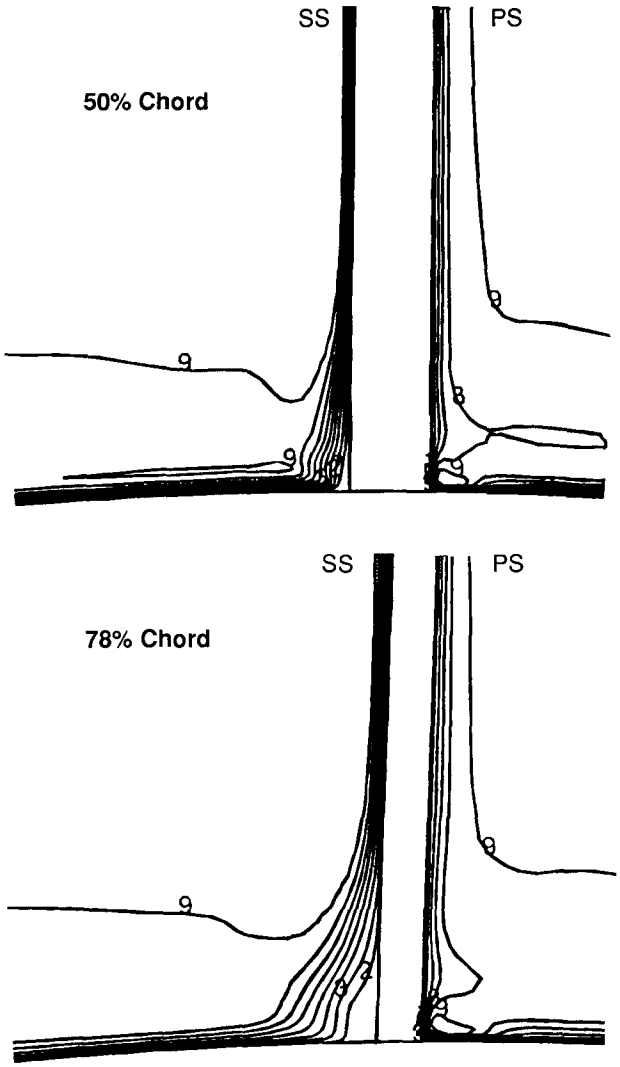

Fig. 11: No clearance/stationary hub: contours of total pressure $((P_t-P_{tin})/q_{in})$ at different axial stations for smooth wall (contour 1 = -1.0, contour 9 = -0.2, contour increment = 0.1)

Figure 11, also for the no clearance, stationary hub, shows the total pressure coefficient at two axial situations, 50% and 78% of blade chord. The quantity plotted is the difference between the local total pressure and the total pressure averaged over the entire inlet, divided by the average inlet dynamic pressure ($(P_t - P_{tin})/q_{in}$), with each contour one tenth the mean dynamic pressure. The lower 25% of the span and roughly 90% of a blade pitch are shown.

The figure indicates the axial development of the endwall corner flow and the build-up of low total pressure fluid on the suction surface near the hub due, in part, to the migration of boundary layer fluid on the hub to the suction surface. (For reference, the hub boundary layer thickness at inlet is roughly 2% span.) Examination of the streamlines near the blade surface showed little migration of boundary layer fluid down the span, with the larger part of the accumulation of low momentum fluid in the suction corner from the endwall flow across the passage.

No Clearance/Smooth Wall/Moving Hub

The solution for no clearance and a *moving* end wall at the hub was also examined to assess the effects of wall motion on the flow in

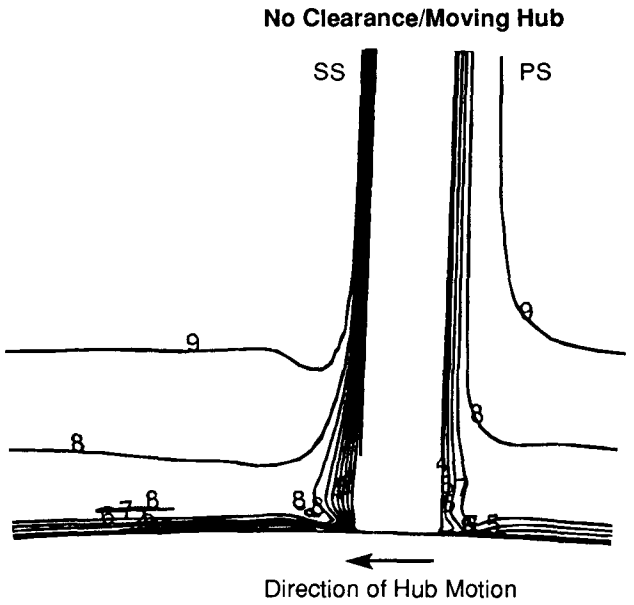

Fig. 12: No clearance/moving hub: contours of total pressure $((P_t-P_{tin})/q_{in})$ at 50% chord for smooth wall (contour 1 = -1.0, contour 9 = -0.2, contour increment = 0.1)

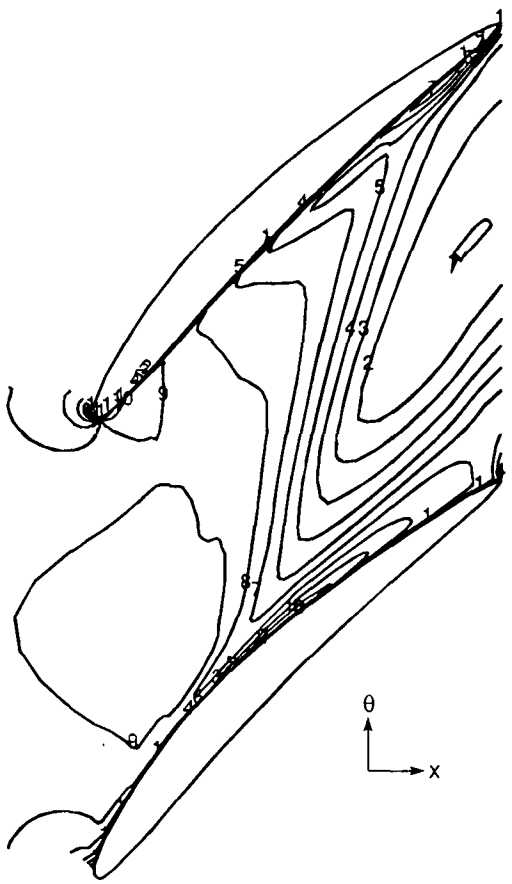

Fig. 13: Contours of axial velocity $(C_x/\overline{C}_x)$ on 2.4% span constant radius surface, with clearance/smooth wall/moving hub (contour 1 = 0.0, contour 11 = 1.0, contour increment = 0.1)

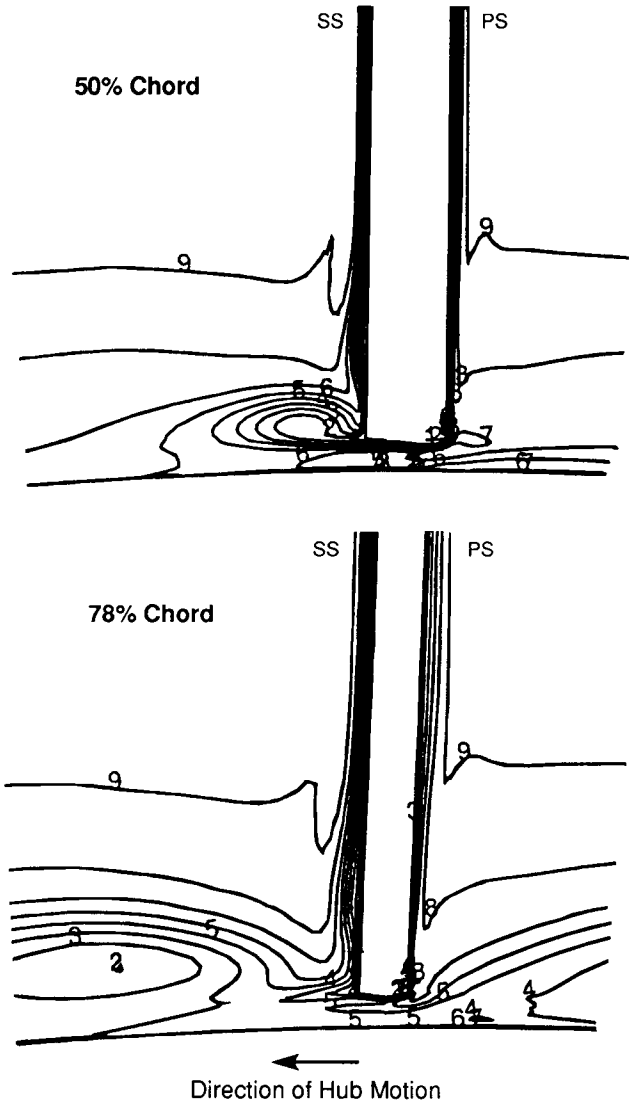

Fig. 14: Clearance/moving hub: contours of total pressure ($(P_t-P_{tin})/q_{in}$) at different axial stations (contour 1 = -1.0, contour 9 = -0.2, contour increment = 0.1)

the endwall region. Figure 10b, which presents contours of axial velocity ($C_x/\overline{C_x}$) at the 2.4% span radial location, can be compared directly to Fig. 10a for a stationary wall. Figure 12 presents contours of total pressure at the 50% chord location and can be compared to the results for this location in Fig. 11. The comparisons show that the moving wall causes little change in overall flow features. More specifically, the changes that occur between moving and stationary walls will be demonstrated to be small compared to those due to clearance (to be discussed below). The principal change with a moving wall is the existence of a small region near the hub with higher energy fluid, presumably resulting from the work done by the moving hub, but the low velocity region near the suction surface corner is still present.

Hub Clearance/Smooth Wall/Moving Hub

Axial Velocity Contours. With clearance, the flow in the endwall region changes markedly. Figure 13, which presents axial velocity normalized by average inlet velocity ($C_x/\overline{C_x}$) on a radial surface at 2.4% span, can be compared directly to the no clearance results in Fig. 10. Higher axial velocities associated with the clearance flow are seen in the midchord region near the blade suction surface. More importantly, the low velocity contours at the rear of the passage are not near the blade but are rather clustered near midpitch, and there is no obvious suction surface separation. As shown in more detail subsequently, we identify these features with the clearance vortex.

Total Pressure Contours. Figure 14 shows the total pressure coefficient for two axial planes at 50% and 78% chord, and can be compared directly with Fig. 11 (or 12). At 50% chord, the suction surface boundary layer near the clearance is thinned due to the clearance flow. Further, the fluid at the edge of the jet which flows through the clearance forms the core of a vortex which can be seen at the left of the blade tip. This core travels away from the blade surface (compare with the low total pressure region at 78% chord in the lower figure), as can be inferred from basic considerations of vortex kinematics (Chen et al., 1991). In addition to motion across the passage, the presence of the vortex implies that higher total pressure fluid from outside the blade surface boundary layer moves down near the suction surface. Evidence of this motion can be seen at both the 50% and 78% locations.

From the calculations, one can see not only that flow through the clearance is the major agent in preventing corner separation (as has been known for some time), but also several other points. One, which was made initially by Storer (1991), is that the leakage jet boundary is the main region of high dissipation, as might be expected because of the high shear. Another point which relates more to the issue of blockage is that the low total pressure fluid appears in the core of a vortex which grows in size as one proceeds downstream. Finally, although corner separation is suppressed with clearance, fluid with high loss and low momentum is still present across much of the passage near the hub.

This last feature may be more apparent in Fig. 15. In this figure, the grey surface in the upper right corner is the suction surface of the blade from midchord to trailing edge. A neighboring blade is shown to the left. The trailing edges of the blades are in the foreground and the hub is outlined in black. Roughly the lower 25% of the passage (at the exit) is shown. The view is looking at the exit plane of the passage from downstream.

The large surface in the upper portion of the figure is an axial station at 50% chord on which are displayed levels of total pressure. The color scale in terms of the total pressure loss coefficient ranges from red ($(P_t-\overline{P_{tin}})/q_{in} \sim 0$) to blue ($(P_t-\overline{P_{tin}})/q_{in} \sim -0.8$). The other colored plane surface is at 78% chord, and includes only the lower 8% of the blade span. The low total pressure region associated with the clearance flow is seen even at 50% chord, but at 78% chord this has grown to occupy much of the endwall region. In the figure, the lowest total pressure fluid is outlined somewhat arbitrarily by a rectangle, which will be referred to as the "high loss rectangle" in what follows. At both these planes, the lowest total pressure is not on the wall but rather at the center of the leakage vortex.

Particle Paths. To examine the source of the high loss fluid, particles were released in the lowest total pressure region at 50% chord and tracked forward and backward along streamlines. The paths integrated forward intersected the high loss rectangle at 78% chord, verifying that the particle paths tracked the regions of low total pressure. Particle paths integrated backward came from the region where the tip leakage jet left the clearance gap.

To illustrate the last point, particle paths originating from a position two computational cells (0.2% span) underneath the blade are displayed in Fig. 16. The orientation of the view into the blade passage is similar to Fig. 15 and the particle paths have been followed past the axial position of the high loss rectangle at 78% chord to the blade trailing edge plane. The blue paths, which originate from the

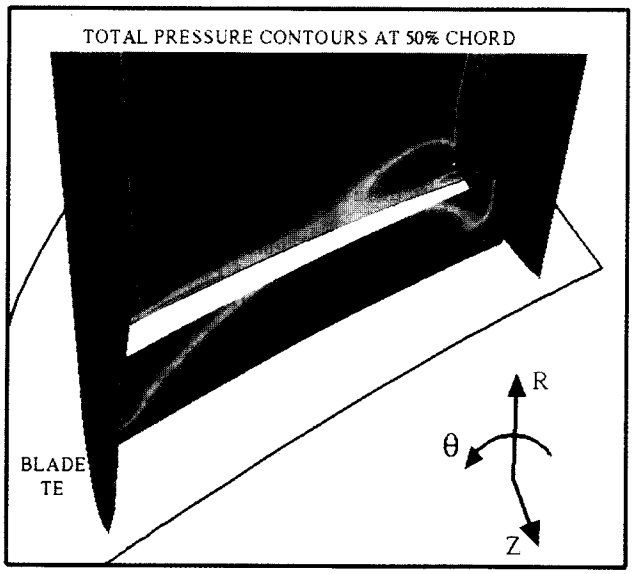

Fig. 15: Total pressure contours in the passage with smooth wall; contour planes at axial locations of 50% and 78% chord, view from rear of passage

first 40% of the blade chord, show helical trajectories because these particles spiral around the vortex core before passing through the high loss rectangle. The red paths, which originate from 50% to 78% of the chord, encircle the loss rectangle. Particles released from two cells below the blade tip over the last 20% of the chord are colored green in the figure. These convect across the passage, ending up at radial positions higher than the blade gap. The boundary that the green and red particles make at blade row exit has a shape similar to the boundary of the low total pressure fluid at that axial location (shown in Fig. 15 by the plane of data at 78% chord).

These particle paths indicate that the low total pressure has not been removed from the flow, but rather transported by the clearance flow and vortex across the endwall region. Moreover, the computations show that loss has been generated by the shear flow emerging from the blade tip and, to a smaller extent, by mixing in the vortical region, and the overall loss in the endwall region is more than that of the no-clearance case. The particle tracking showed that the high loss fluid is located in the vortex core. Further, the high loss region is near the suction side of the blade where the jet exits; particles that end up in the central part of the core come principally from the edge of the clearance jet, as seen in Fig. 15.

The clearance flow is thus a primary contributor to loss and the existence of low total pressure fluid in the passage. Further, although the discussion so far is in terms of loss, it is not much of a stretch to connect the regions of high loss with high blockage as well. While these regions can be linked to low streamwise and axial velocity in the endwall, they have not been determined conclusively to be the cause of the stall in the experiment. It is observed, however, that as incidence is increased, the high loss, low velocity region which is located in the vortex core grows substantially. Also, the clearance flow velocity increases in the direction perpendicular to the blade stagger line, resulting in larger regions of negative axial velocity in the endwall region, and thus larger blockage.

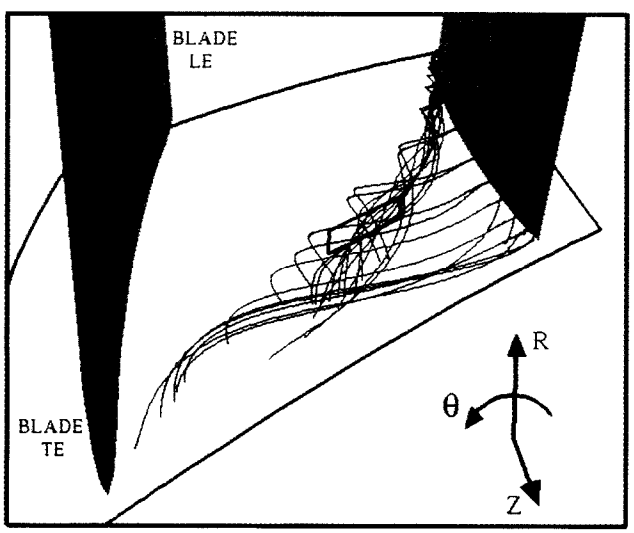

Fig. 16: Particles released from the blade tip, smooth wall; view from rear of passage

HUB TREATMENT

Velocity Vectors

With hub treatment, the flow is qualitatively different as to both streamline pattern and momentum content. Figure 17 displays velocity vectors at two axial stations. The vectors are viewed at an angle 55 degrees from axial; this is roughly the angle that the vortex has as it crosses the passage. The difference in the incoming jet flow angle (in the r-θ plane) at the two stations arises because of the difference in hub outflow velocity; at the 40% location the absolute velocity is almost wholly the hub velocity, whereas at the 10% location the relative outflow velocity from the grooves is near its

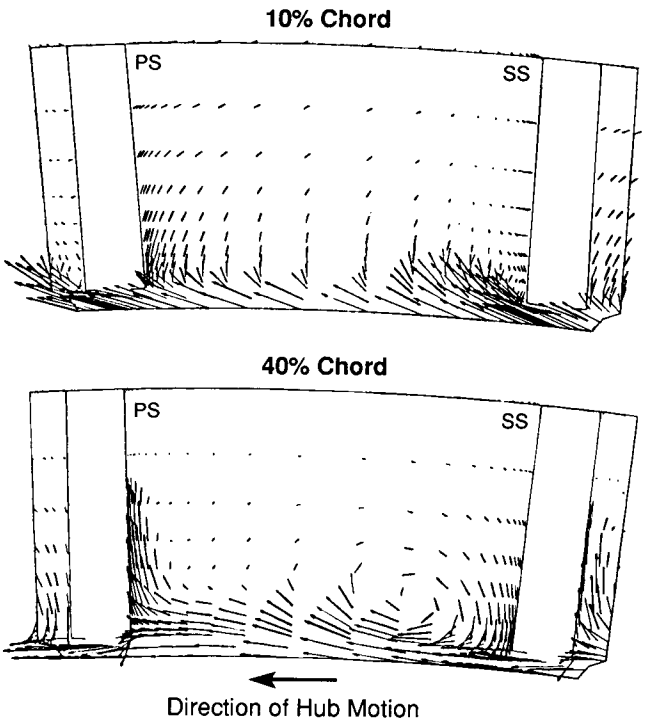

Fig. 17: Hub treatment: velocity vectors at different axial stations; view angle = 55 deg

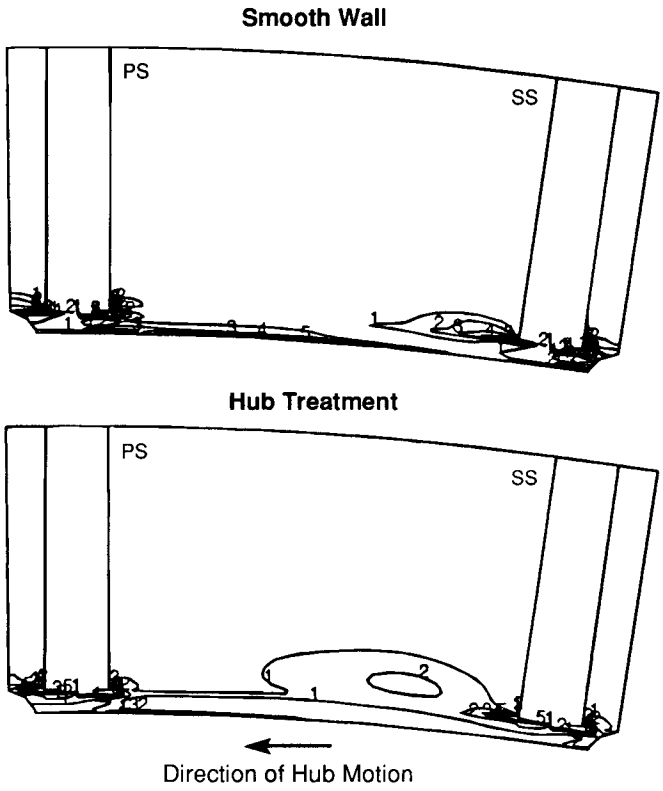

Fig. 18: Contours of streamwise vorticity (ω_s x clearance/$C_{leakage}$) at 40% chord (contour 1 = 0.2, contour 5 = 1.0, contour increment = 0.2)

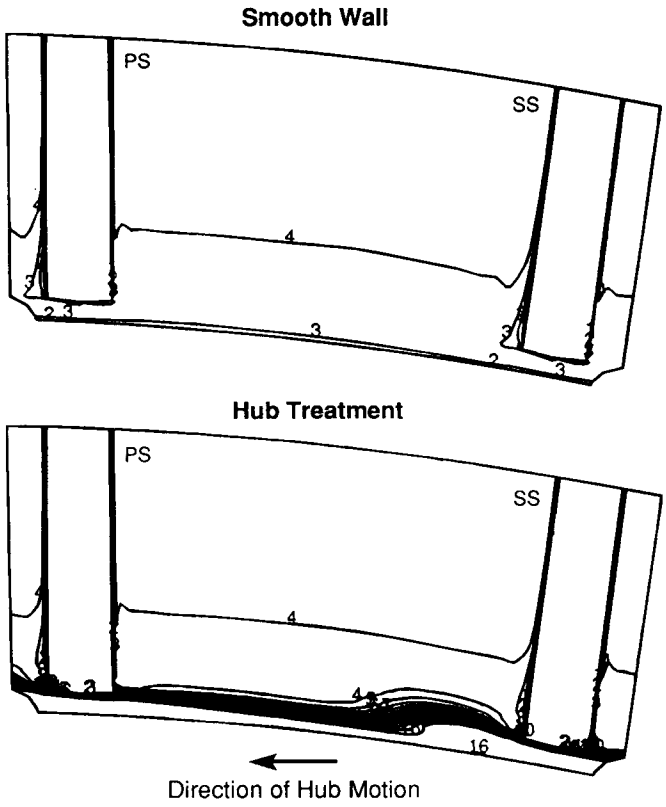

Fig. 19: Total pressure ((P_t-P_{tin})/q_{in}) contours at 10% chord (contour 1 = -1.0, contour 16 = 2.75, contour increment = 0.25)

maximum value. At the 10% chord location, the jet enters from the hub treatment, with a vortex forming near the blade tip at the right of the passage. The vortex center moves away from the blade and the vortex enlarges as it proceeds downstream, as shown in the 40% chord results. At this location, a high velocity flow moves up the pressure surface of the blade at the left of the passage; this originated from the jet shown at the 10% location.

Vorticity Contours

To examine the strength and size of the vortex in a more quantitative fashion, Fig. 18 displays contours of streamwise vorticity at the 40% chord axial station, for both smooth wall and hub treatment. The magnitude of the streamwise vorticity has been non-dimensionalized by the ideal leakage velocity for the smooth wall, $C_{leakage}$, as defined using the mean blade loading, $C_{leakage} = \sqrt{2 \cdot \text{Mean Blade Pressure Difference} / \rho}$ (Chen, 1991) and the tip clearance, τ*. The figure indicates increased secondary circulation with hub treatment compared to smooth wall clearance flow, as one might expect from the high dynamic pressure of the jet. The circulation magnitude obtained from the calculations as well as from the velocity measurements confirm this. Although not shown, at the rear of the passage, the vortex is drawn to the hub and much of the high vorticity fluid is sucked into the treatment.

* This choice of parameters is not totally unequivocal; it amounts to basing the vorticity on a circulation of magnitude, $C^2_{leakage}$ t, where t is the time during which vorticity is produced, spread over an area ($C_{leakage}$ t) τ.

Total Pressure Contours

To demonstrate the effect of hub treatment on the endwall flowfield in a different manner, plots of total pressure loss coefficient at two axial stations are shown for the smooth wall and the hub treatment in Figs. 19 and 20. The station at 10% chord is displayed in Fig. 19. A high total pressure jet emanates from the hub treatment with total pressure several q_{in} higher than the total pressure near the endwall in the smooth wall case.

Figure 20 shows the axial station at 40% chord. With hub treatment, high total pressure fluid from the jet fills the endwall region. The high total pressure fluid from the jet is also found near the pressure surface, moving away from the endwall. With the smooth wall, the high loss (and high blockage) area associated with the clearance vortex has started to form. With the hub treatment, there is no low total pressure vortex core because the high pressure jet emerging from the hub treatment upstream of this axial station has washed the blade tip and removed (through mixing) the low total pressure fluid.

The total pressure loss coefficient at 78% chord is displayed in Fig. 21. For the smooth wall, the region with appreciable loss (say greater than 0.5 q_{in}) takes up much of the passage in the endwall region. With the hub treatment, however, this area is occupied by fluid with an excess of total pressure. The suction at the rear of the treatment draws this high total pressure fluid down to the hub. At the right of the passage, the suction also draws low total pressure fluid from the suction side of the blade into the tratment. At the left of the passage, high total pressure fluid which originated from the treatment jet at the front of the passage can be seen near the pressure surface of the blade moving away from the endwall. This fluid emerges as a jet at the rear of the passage (Cheng et al., 1984) and contributes little to the elimination of the blockage.

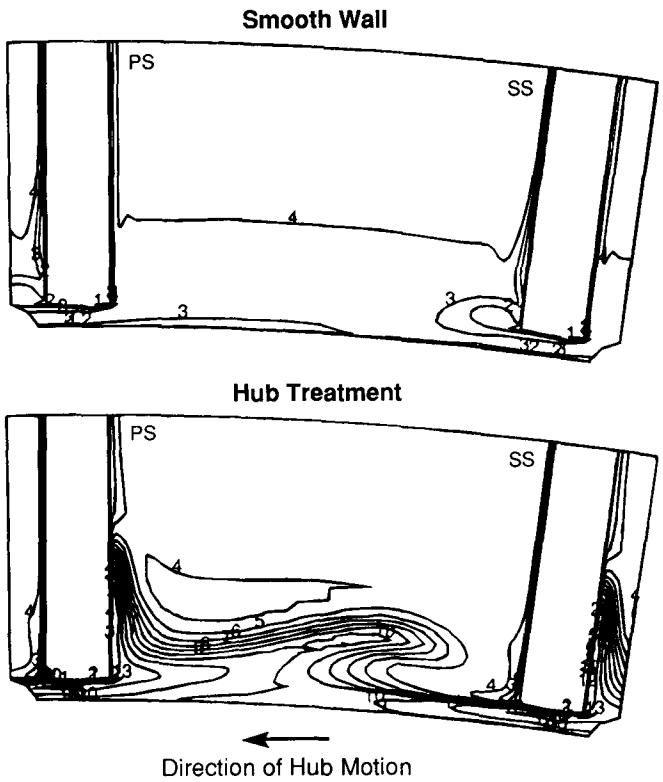

Fig. 20: Total pressure ($(P_t-P_{tin})/q_{in}$) contours at 40% chord (contour 1 = -1.0, contour 13 = 2.0, contour increment = 0.25)

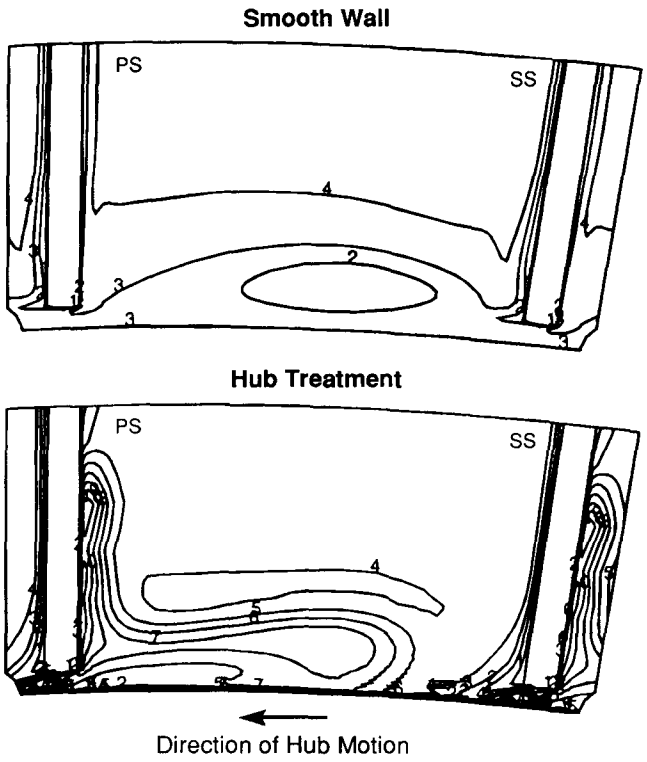

Fig. 21: Total pressure ($(P_t-P_{tin})/q_{in}$) contours at 78% chord (contour 1 = -1.0, contour 10 = 1.25, contour increment = 0.25)

To examine the roles of treatment jet, suction, and leakage flow from another perspective, particle paths in the 3-D flowfield are displayed in Fig. 22. The particles are released on the hub roughly bounding the region of higher total pressure fluid coming from the treatment at 10% to 15% axial chord. The view is looking down the blade passage with the leading edge of one blade at the center of the figure, the neighboring blades invisible, and approximately the lower 40% of the blade span shown. A contour plot of total pressure is shown on a plane at the trailing edge location with low total pressure indicated by blue and high total pressure by red. The particles are marked with two different colors to show the release position; red particles were released over the central 50% of the pitch and blue particles over the rest. The computations show that the groups follow qualitatively different trajectories. Most of the red particles cross the passage, impact the pressure surface of the blade, and move up this surface away from the endwall. The blue particles, however, take helical paths, moving back towards the endwall. The hub treatment, therefore, does not suppress the vortex, but its core is now a region of high, rather than low, total pressure fluid.

Blockage

The action of the treatment has been described so far in terms of the streamlines and total pressure, but a quantity more directly related to endwall stall is blockage. The effect of the hub treatment on blockage in the passage is illustrated by Fig. 23, which presents contour plots of the component of velocity along the blade stagger line (velocity component along the (45 degree) stagger line/$\overline{C_x}$), at the 78% chord location for smooth wall and for hub treatment. The velocity component in the stagger direction is used as a crude indication of the flow "along" the blade passage; other components can also be examined, but the message is similar.

The velocity plots are similar to those of total pressure. For the smooth wall they show a mid-passage region of low velocity (all contours with number less than 6 have velocity less than the mean axial velocity) and consequently large stream tube area increase. For the hub treatment, this low velocity, high blockage, region does not exist. In fact the highest velocity occurs roughly in the region that was occupied by the low velocity fluid with the smooth wall, but is now occupied by high total pressure fluid that emerged from the front of

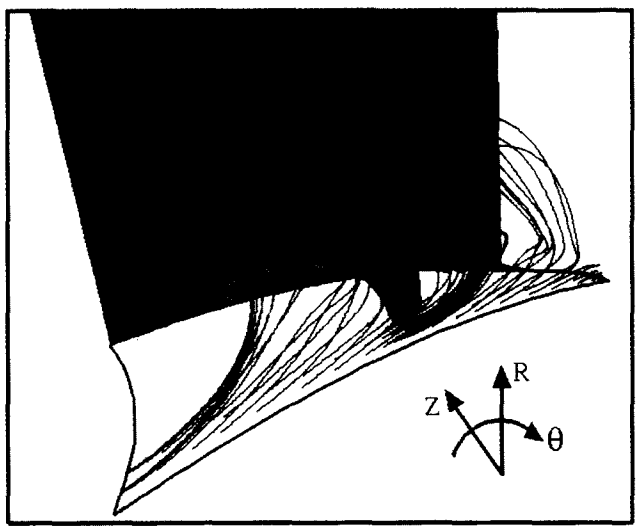

Fig. 22: Hub treatment: particles released in treatment jet; view from upstream looking downstream

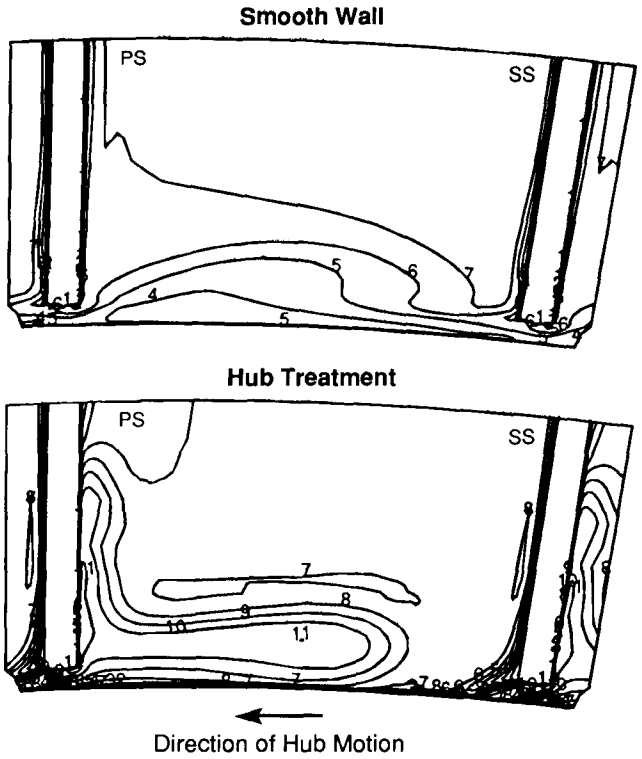

Fig. 23: Contours of velocity along stagger line ($C_{stagger}/\overline{C}_x$) at 78% chord (contour 1 = 0.0, contour 11 = 2.0, contour increment = 0.2

the treatment grooves. Again, on the right side of the passage the treatment suction can be seen to be removing low velocity fluid.

Figure 23 is a demonstration of the combined effects of the casing treatment. There is a region of high velocity due to the injection. In the aft part of the passage, this high velocity region is moved closer to the endwall by the suction that occurs there; this suction is also capable of removing high blockage fluid from the rear of the passage.

As a final note on the operation of hub and casing treatment portrayed here, we can make some comments on the relation of this work to high speed compressors. The computations of Adamczyk et al. (1991) strongly suggest that the leakage flow is also an important feature of stall onset in high speed machines, i.e. compressors in which the pressure rise due to a shock is appreciable. In particular, that study showed a build up of low total pressure fluid along the endwall due to the interaction of the leakage vortex and the passage shock. It thus appears that many features of the stall problem may carry over from low speed to high speed and that, in particular, injection of high energy fluid in the forward part of the the blade passage endwall to reduce or eliminate the growth of the regions of low total pressure would have a beneficial effect on flow range.

SUMMARY AND CONCLUSIONS

1. Computations have been carried out of the flow in the endwall region of a compressor blade row, with a smooth and a grooved endwall.
2. Comparison with velocity field measurements in a highly loaded cantilevered stator/rotating hub configuration shows that the computations provide a description that is useful for obtaining insight into the general features of the flow structure.
3. The computations show that the tip leakage and resulting vortex are dominant features of the endwall flow. The region of high loss and high blockage which is found near midpitch (rather than near the blades) is associated directly with the leakage flow.
4. First-of-a-kind computations have been carried out with blowing and suction through the hub to simulate the types of casing treatment which have been most successful in suppressing stall.
5. The computations show that there are two main actions of hub or casing treatment on the leakage flow: 1) suction of the low total pressure fluid at the rear of the passage, and 2) suppression of the blockage in the core of the leakage vortex due to the energizing of the leakage flow by high velocity injection at the front of the passage. In the latter, it is also shown that 50% or less of the treatment flow is useful in accomplishing this, the rest being dissipated with little effect on the endwall characteristics.

ACKNOWLEDGEMENTS

Support for the part of this work carried out at MIT was provided by Allison Gas Turbine Division of General Motors. This support, and the interest, strong encouragement, and helpful comments of Dr. R.A. Delaney and Mr. P.C. Tramm of Allison, are gratefully acknowledged. In addition, the authors express their appreciation for the many useful discussions with Mr. A. Khalid, the constructive critiques of Professor N.A. Cumpsty, and the efforts of Ms. D.I. Park in the preparation of the manuscript. We also wish to acknowledge the help given by T.A. Beach, M.L. Celestina, K. Kirtley, and R.A. Mulac in carrying out the computations.

REFERENCES

Adamczyk, J.J., Celestina, M.L., Beach, T.A., Barnett, M., 1989, "Simulation of Three-Dimensional Viscous Flow Within a Multi-Stage Turbine," *ASME Journal of Turbomachinery*, Vol. 112, No. 3, pp. 370-376.

Adamczyk, J.J., Celestina, M.L., Greitzer, E.M., 1991, "The Role of Tip Clearance in High-Speed Fan Stall," ASME Paper 91-GT-83, 1991 ASME International Gas Turbine Conference.

Baldwin, B., Lomax, H., 1978, "Thin Layer Approximation and Algebraic Model for Separated Turbulent Flows," AIAA Paper 78-257.

Chen, G.-T., Greitzer, E.M., Tan, C.S., Marble, F.E., 1991, "Similarity Analysis of Compressor Tip Clearance Flow Structure," *ASME Journal of Turbomachinery*, Vol. 113, pp. 260-271.

Cheng, P., Prell, M.E., Greitzer, E.M., Tan, C.S., 1984, "Effects of Compressor Hub Treatment on Stator Stall Margin and Performance," *Journal of Aircraft*, Vol. 21, No. 7, pp. 469-475.

Crook, A., 1989, "Numerical Investigation of Endwall/Casing Treatment Flow Phenomena," MIT GTL Report No. 200.

Dawes, W.N., 1987, "A Numerical Analysis of the Three-Dimensional Viscous Flow in a Transonic Compressor Rotor and Comparison with Experiment," *ASME Journal of Turbomachinery*, Vol. 109, pp. 83-90.

Dong, Y., Gallimore, S.J., Hodson, H.P., 1986, "Three-Dimensional Flows and Loss Reduction in Axial Compressors," ASME Paper 86-GT-193.

Fujita, H., Takata, H., 1984, "A Study of Configurations of Casing Treatment for Axial Flow Compressors," *Bulletin of the JSME*, Vol. 27, No. 230, pp. 1675-1681.

Greitzer, E.M., Nikkanen, J.P., Haddad, D.E., Mazzawy, R.S., Joslyn, H.D., 1979, "A Fundamental Criterion for the Application of Rotor Casing Treatment," *ASME Journal of Fluids Engineering*, Vol. 101, pp. 237-243.

Hah, C., 1986, "A Numerical Modelling of Endwall and Tip Clearance FLow of an Isolated Compressor Rotor," *ASME Journal of Engineering for Power*, Vol. 108, pp. 15-21.
Jameson, A., Schmidt, W., Turkel, E., 1981, "Numerical Solutions of the Euler Equations by Finite Volume Methods Using Runge-Kutta Time-Stepping Schemes," AIAA-81-1259.
Johnson, M.C., 1985, "The Effects of Hub Treatment on Compressor Endwall Flowfields," M.S. Thesis, Dept. of Aeronautics and Astronautics, MIT.
Lee, N.K.W., 1990, "Effects of Compressor Endwall Suction and Blowing on Stability Enhancement," MIT GTL Report No. 192, January 1988; see also *ASME Journal of Turbomachinery*, Vol. 112, pp. 133-144.
McDougall, N.M., 1988, "Stall Inception in Axial Compressors," Ph.D. Thesis, Engineering Department, Cambridge University.
Pouagare, M., Delaney, R.A., 1986, "Study of Three-Dimensional Viscous Flows in an Axial Compressor Cascade Including Tip Leakage Effects Using a SIMPLE-Based Algorithm," *ASME Journal of Turbomachinery*, Vol. 108, pp. 51-58.
Prince, D.C., Jr., Wisler, D.C., Hilvers, D.E., 1974, "Study of Casing Treatment Stall Margin Improvement Phenomena," NASA CR-134552.
Smith, G.D.J., Cumpsty, N.A., 1985, "Flow Phenomena in Compressor Casing Treatment," *ASME Journal of Engineering for Gas Turbines and Power*, Vol. 107, pp. 532-541.
Storer, A., 1991, "Tip Clearance Flow in Axial Compressors," Ph.D. Thesis, Dept. of Engineering, Cambridge University.
Takata, H., Tsukuda, Y., 1977, "Stall Margin Improvement by Casing Treatment – Its Mechanism and Effectiveness," *ASME Journal of Engineering for Power*, Vol. 99, pp. 121-133.

APPENDIX A: COMPUTATIONAL PROCEDURE

GOVERNING EQUATIONS AND BOUNDARY CONDITIONS

The equations that govern the steady viscous flow in three dimensions, along with the equation of state, form the system to be solved. The scheme used is finite volume-cell centered and second order accurate in space for a smooth uniform mesh. The discretized system of equations has unstable properties and can exhibit odd-even point decoupling. To suppress these instabilities, artificial dissipation terms made up of second and fourth difference smoothing operators are added to the equations. The time stepping scheme used to fully discretize the system is a four-stage Runge-Kutta integration. Local time stepping for each cell and residual averaging is used to accelerate the convergence. A solution was deemed convergent when the average of the density time derivative over the domain had fallen two to three orders of magnitude from the initial value. Turbulent stresses are simulated using the model of Baldwin and Lomax (1978). The artificial dissipation is modified by a Mach number scaling to remove its influence on the regions of the flowfield in which viscous effects are dominant.

With subsonic inlet and exit regions four conditions must be set at the upstream boundary and one at the downstream boundary. Stagnation pressure and temperature were specified at the inlet as well as the flow angles in the z-θ and r-θ planes. The inlet axial velocity is set with a characteristic equation as is usual in this procedure. For the downstream boundary, the static pressure at the hub is set and simple radial equilibrium is held. For solid wall boundaries, no slip conditions were held at all surfaces.

COMPUTATIONAL GRIDS

For both the viscous and inviscid solutions, an axisymmetric algebraic H-type mesh is generated. Table A.1, containing pertinent information about the grids, is shown below.

TABLE A.1
GRID CONFIGURATIONS

Number of Grid Points	Viscous Grid	
	Hub Clearance	No Hub Clearance
Blade to Blade	49	41
Hub to Tip	47	33
Hub to Gap	9	---
Inlet to Exit	111	89
L.E. to T.E.	56	44

Figure A.1 shows an r-θ plane at the midchord of the grid used in the calculations. The lower third of the blade passage is shown to emphasize the grid in the gap region underneath the tip of the blade. The grid was formed in this manner to resolve the flow in the gap region; however, grid distortion (shear) is introduced in the gap near the blade tip. Because of concern that grid shear might introduce errors in the flowfield solution, an investigation of the effect of grid shear on the solution was carried out. As reported by Crook (1989), the conclusion is that there is no strong effect of the shear on the tip flow solution.

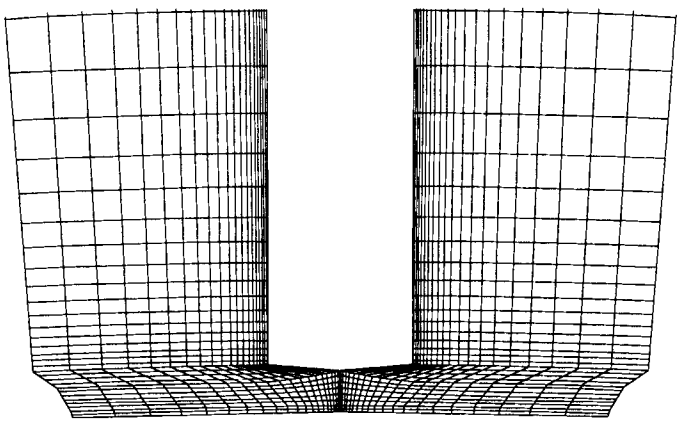

Fig. A.1: Viscous computation grid at midchord location; lower fifth of blade shown